Acta Crystallographica Section D
Biological Crystallography
ISSN 0907-4449

Structure at 1.5 Å resolution of cytochrome c_{552} with its flexible linker segment, a membrane-anchored protein from *Paracoccus denitrificans*

Chitra Rajendran,[a]* Ulrich Ermler,[a] Bernd Ludwig[b] and Hartmut Michel[a]

[a]Max Planck Institute of Biophysics, Max-von-Laue-Strasse 3, 60438 Frankfurt am Main, Germany, and [b]Johann Wolfgang Goethe University, Max-von-Laue-Strasse 9, 60438 Frankfurt am Main, Germany

Correspondence e-mail: chitra.rajendran@psi.ch

Received 18 April 2010
Accepted 24 May 2010

PDB Reference: cytochrome c_{552}, 3m97.

Electron transfer (ET) between the large membrane-integral redox complexes in the terminal part of the respiratory chain is mediated either by a soluble *c*-type cytochrome, as in mitochondria, or by a membrane-anchored cytochrome *c*, as described for the ET chain of the bacterium *Paracoccus denitrificans*. Here, the structure of cytochrome c_{552} from *P. denitrificans* with the linker segment that attaches the globular domain to the membrane anchor is presented. Cytochrome c_{552} including the linker segment was crystallized and its structure was determined by molecular replacement. The structural features provide functionally important information. The prediction of the flexibility of the linker region [Berry & Trumpower (1985), *J. Biol. Chem.* **260**, 2458–2467] was confirmed by our crystal structure. The N-terminal region from residues 13 to 31 is characterized by poor electron density, which is compatible with high mobility of this region. This result indicates that this region is highly flexible, which is functionally important for this protein to shuttle electrons between complexes III and IV in the respiratory chain. Zinc present in the crystallization buffer played a key role in the successful crystallization of this protein. It provided rigidity to the long negatively charged flexible loop by coordinating negatively charged residues from two different molecules and by enhancing the crystal contacts.

1. Introduction

Aerobic respiration is a vital process in biology. Several membrane-spanning protein complexes (complexes I, III and IV) build up a proton gradient across the cell membrane that is driven by exothermic redox processes with NADH as the electron donor and O_2 as the terminal electron acceptor. Electron transfer between the protein complexes is mediated by either quinones or cytochrome *c*. Cytochrome *c* molecules function as electron carriers in diverse physiological contexts and are found with one or more haem C moieties, as a soluble form or membrane-anchored and sometimes also as part of a multisubunit complex.

Our interests are directed to cytochrome *c* molecules that shuttle electrons from the cytochrome bc_1 complex (complex III) to cytochrome *c* oxidase (complex IV); we have therefore focused on the membrane-anchored cytochrome c_{552} from the soil bacterium *Paracoccus denitrificans*.

Architecturally, cytochrome c_{552} is organized as a tripartite structure containing (i) an N-terminal hydrophobic membrane-spanning segment that functions as a membrane anchor (30 residues), (ii) a highly negatively charged linker segment (40 residues) and (iii) a typical class I cytochrome domain (100 residues). The latter is characterized by the presence of a haem C moiety that is covalently linked to the polypeptide *via* two thioether bonds with cysteines and two axial ligands: a histidine and a methionine. Truncated forms of the protein, cytochrome c_{552} fragment A (the cytochrome *c* domain only), fragment B (the cytochrome *c* domain and the highly negatively charged segment) and the full-length protein (the cytochrome *c* domain, the highly negatively charged region and the membrane anchor), have been produced in *Escherichia coli* (Reincke *et al.*, 1999). The structure of fragment A has been determined by X-ray crystallography (Harrenga *et al.*, 2000).

Table 1
Data-collection and refinement statistics.

Values in parentheses are for the highest resolution shell.

Wavelength (Å)	0.97858
Space group	$P2_12_12_1$
Unit-cell parameters (Å, °)	a = 37.385, b = 39.036, c = 92.947, $\alpha = \beta = \gamma = 90$
Resolution range (Å)	30–1.5 (1.55–1.50)
Total No. of reflections	64914
No. of unique reflections	20882
Completeness (%)	93.2 (82.6)
$R_{\rm merge}$† (%)	5.8 (25.5)
Refinement statistics	
No. of water molecules	226
$R_{\rm cryst}$ (%)	25
$R_{\rm free}$ (%)	26
Resolution range (Å)	30–1.5
R.m.s. deviation from ideality‡	
Bonds (Å)	0.028
Angles (°)	2.4

† $R_{\rm merge} = \sum_{hkl}\sum_i |I_i(hkl) - \langle I(hkl)\rangle| / \sum_{hkl}\sum_i I_i(hkl)$, where $I_i(hkl)$ is the intensity measurement for a given reflection and $\langle I(hkl)\rangle$ is the average intensity for multiple measurements of this reflection. ‡ With respect to Engh and Huber parameters (Engh & Huber, 1991).

In the bacterial membrane, cytochrome c_{552} appears to be associated with cytochrome *c* oxidase and the bc_1 complex, forming a supramolecular complex (Berry & Trumpower, 1985; Turba *et al.*, 1995). Subfractionation of the ternary complex revealed that the membrane-bound cytochrome c_{552} is more tightly bound to the cytochrome *c* oxidase than to the bc_1 complex. However, the structural basis of the interaction between cytochrome c_{552} and its interacting partners is unknown as no complex structures have been determined. It has long been appreciated that electrostatic forces govern the interaction of cytochrome *c* with its supracomplex partners. Accordingly, the positively charged lysine residues on the surface of cytochrome c_{552}, which are clustered around the exposed heme edge and the negatively charged patches above the binuclear Cu_A center in subunit II, provide the basis for this electrostatic interaction (Witt *et al.*, 1998). According to site-directed mutagenesis studies, Trp121, which is present at the contact surface of cytochrome *c* oxidase subunit II, plays a crucial role in mediating electron transfer from the cytochrome c_{552} haem to the Cu_A centre, which is the first electron acceptor in the oxidase (Witt *et al.*, 1998; Zhen *et al.*, 1999). Furthermore, the results of fast kinetic and mutagenesis studies suggest that the encounter complex between the cytochrome bc_1 complex and cytochrome c_{552} is guided primarily by the overall electrostatic surface potential rather than by defined charges (Janzon *et al.*, 2008).

It has been speculated that the soluble fragment B acts as a swivel arm for the shuttling of electrons between the redox partners. The presented crystal structure of fragment B provides evidence for the flexibility of the negatively charged stretch.

2. Materials and methods

2.1. Purification

The gene encoding cytochrome c_{552} fragment B of *P. denitrificans* was cloned and expressed in the BL21 (DE3) strain as reported previously (Reincke *et al.*, 1999). For purification, fragment B was loaded onto a Q-Sepharose ion-exchange column using a buffer solution consisting of 50 m*M* Tris–HCl, 1 m*M* EDTA pH 7.0 and was eluted with a salt gradient of 100–400 m*M* NaCl in the same buffer. Subsequently, the pooled fractions were subjected to gel filtration (Sephacryl S-200 column) with Tris–EDTA buffer pH 7.0 containing 100 m*M* NaCl.

2.2. Crystallization

Fragment B of cytochrome c_{552} was concentrated to 10 mg ml^{-1} in 50 m*M* Tris–HCl buffer pH 7.0 and crystallized using the sitting-drop vapour-diffusion method. We applied commercial screening solutions including those from Hampton Research and Jena Biosciences and self-made sparse-matrix screens consisting of various PEGs at varying concentrations and different pH values. Crystals suitable for X-ray crystallography appeared within two weeks using a reservoir buffer consisting of 20% PEG 550 MME and 0.1 *M* zinc sulfate at 291 K. Despite considerable efforts, the size of the rod-shaped crystals did not increase beyond 20–50 µm. Crystallization trials without zinc did not yield any crystals.

2.3. Data collection

For data collection, a single crystal was flash-frozen at 100 K in a liquid-nitrogen stream after transferring the crystals into reservoir buffer supplemented with 15% glycerol. A native data set was collected to a resolution of 1.5 Å from a single crystal on beamline PX II at the Swiss Light Source (SLS). All data were indexed, integrated and scaled using *DENZO* and *SCALEPACK* from the *HKL* suite of programs (Otwinowski & Minor, 1997). The space group was $P2_12_12_1$, with unit-cell parameters a = 37.4, b = 39.0, c = 92.9 Å. The volume-to-mass ratio $V_{\rm M}$ of 2.3 Å^3 Da^{-1} and the corresponding solvent content of 46.5% suggested the presence of one molecule per asymmetric unit ($M_{\rm r}$ = 14.4 kDa). Data-collection and processing statistics are listed in Table 1.

2.4. Structure determination and refinement

The initial set of phases for structure determination was obtained by molecular replacement using the program *EPMR* (Kissinger *et al.*, 1999). The structure of soluble fragment A of cytochrome c_{552} from *P. denitrificans* (Harrenga *et al.*, 2000) was used as a search model. The resulting correlation coefficient was 0.41 and the initial *R* factor was 50%. Manual model building was carried out using *XtalView*/*Xfit* (McRee, 1993). Residues 13–31 were not identifiable in the poor

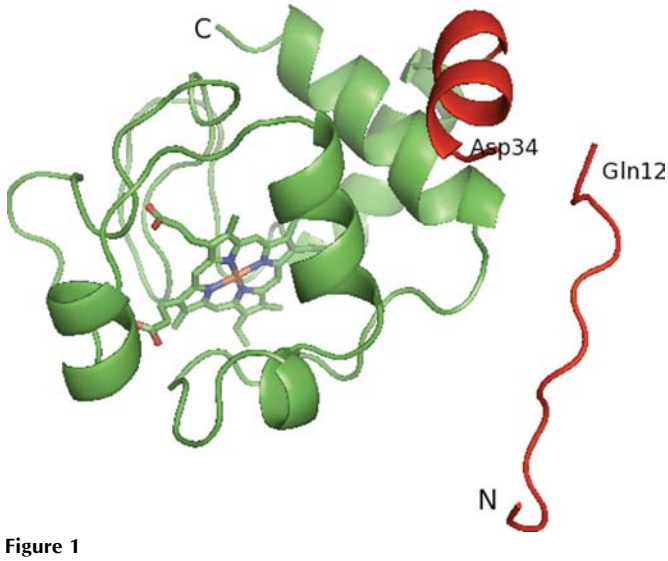

Figure 1
Ribbon plot of fragment B of cytochrome c_{552} from *P. denitrificans*. The haem prosthetic group is depicted as a stick model. The small helix (residues 34–41) and the loop region (residues 1–12) are shown in red and the globular cytochrome domain is shown in green. The amino-terminus and carboxy-terminus are labelled N and C. The disordered residues 13–33 are not shown. This figure was created with *PyMOL* (DeLano, 2008).

Table 2
Zinc-binding sites, coordinating atoms and the distances between them.

Symm, amino acid from the symmetry-related molecule; HOH, water.

Zn1	Symm His3 NE2 (1.99 Å)	Symm Asp88 OD1 (1.98 Å)	Glu100 OE2 (1.95 Å)	Glu104 OE1 (1.98 Å)
Zn2	Glu127 OE1 (1.98 Å)	Glu8 OE2 (1.72 Å)	His10 ND1 (2.03 Å)	Symm Asp82 (1.98 Å)
Zn3	His69 NE2 (2.03 Å)	Symm Glu9 OE2 (2.27 Å)	HOH 199 OH2 (2.23 Å)	HOH 334 OH2 (2.36 Å)
Zn4	His93 NE2 (2.07 Å)	Symm Glu6 OE2 (2.00 Å)	Symm Met1 N (2.14 Å)	Symm Met1 O (1.55 Å)

electron density observed in this region. Four large peaks in the electron-density map were interpreted as Zn^{2+} ions as zinc sulfate was present in the crystallization buffer. Refinement was started with *CNS* v.1.1 (Brünger *et al.*, 1998) using the standard slow-cooling protocol. The R_{free} factor was calculated from 5% of the measured data that were not used in refinement. Model building was performed using *XtalView* (McRee, 1993) and water molecules were included if spherical peaks were greater than 3σ in the $F_o - F_c$ difference electron-density maps. Further positional and *B*-factor refinement was carried out with *REFMAC*5 (Murshudov *et al.*, 1997) and the crystallographic R_{cryst} and R_{free} values for the final model were 25% and 26%, respectively. The *R* and R_{free} factors did not converge below this value even though the resolution was very high. The reason could be that the electron density for residues 13–31 was poor and could not be modelled. The refinement statistics and quality of the final model are summarized in Table 1. The final model contained 226 water molecules. The stereochemical quality of the structure was examined with *PROCHECK* (Laskowski *et al.*, 1993) and *WHAT_CHECK* (Hooft *et al.*, 1996). There were no residues in the disallowed region of the Ramachandran map.

MGHG AEGEEHAQAY TYPVESAGGA EGEAVDEGPD FATVLASADP
AAGEKVFGKC KACHKLDGND GVGPHLNGVV GRTVAGVDGF
NYSDPMKAHG GDWTPEALQE FLTNPKAVVK GTKMAFAGLP
KIEDRANLIA YLEGQQ

Figure 2
Primary sequence of fragment B of cytochrome c_{552} from *P. denitrificans*. The residues are represented in single-letter code. The residues (1–12) in red belong to the loop region, the residues in green (13–32) are disordered in the structure (no electron density was observed), the residues in blue (34–41) form the small helix and the residues in black (42–140) belong to the typical class I cytochrome domain (numbering 2–100 as per PDB code 1ql4; Harrenga *et al.*, 2000).

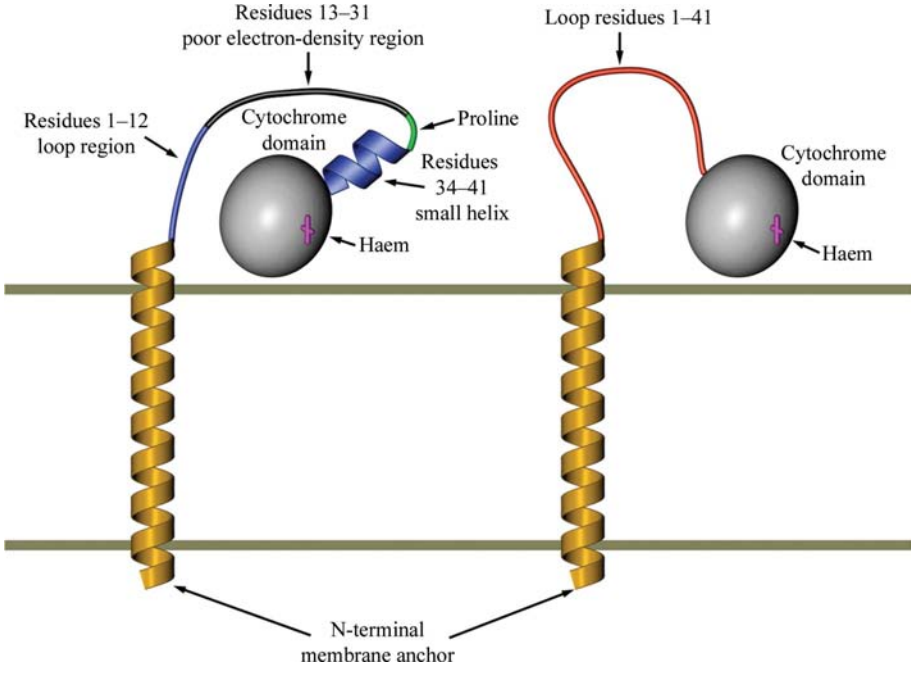

Figure 3
Schematic representation of cytochrome c_{552}. Left: the new model demonstrates the presence of a short helix, thus leading to a shorter loop region than the previously suggested model. Right: the previously suggested model. The grey sphere corresponds to the previously published cytochrome *c* domain, the transmembrane helix is a simulation (structure not known), the blue and green parts are the present work and the haem is shown in pink.

3. Results and discussion

3.1. The globular cytochrome *c* domain

An overall view of the crystal structure of fragment B of cytochrome c_{552} from *P. denitrificans* is shown in Fig. 1; the globular domain is shown in green. As expected, the globular domain of the cytochrome *c* domain essentially corresponds to that of fragment A and the r.m.s.d. value for C^{α} atoms is 0.55. Five α-helices (helices 2–6) are wrapped around the central haem in the characteristic manner conserved in the class I cytochromes *c*.

Most of the 226 solvent molecules modelled into fragment B are conserved in the fragment A structure (550 solvent molecules for the four molecules in the asymmetric unit of the latter; Harrenga *et al.*, 2000) and are therefore independent of the different crystal-packing arrangement. Among the many conserved water molecules in cytochromes *c*, the water molecule named HOH 255 (corresponding to Wat125 in horse cytochrome *c*; Bushnell *et al.*, 1990) is of particular importance. An important role is attributed to it in electron transfer by mediating an ionic interaction between the propionate carboxylate of pyrrole ring A and the invariant Arg76.

The haem group of fragment B of cytochrome c_{552} has a geometry identical to that embedded in fragment A (Harrenga *et al.*, 2000). The distances between the two axial ligands His58 and Met118 and the haem C iron are 2.04 and 2.26 Å, respectively. The thioether bond between Cys54 SG and haem C CAB is 1.83 Å in length and that between Cys57 SG and heme C CAC is 2.43 Å. The Fe atom is displaced 0.22 Å out of the porphyrin plane towards the His85 side chain. Pyrrole rings B and C also show minor deviations from the plane probably owing to the thioether linkages.

3.2. The flexible linker segment

Residues 1–40 of fragment B link the globular cytochrome *c* domain and the N-terminal membrane anchor (the latter was absent in the construct used for crystallization). In the crystal structure this region is composed of an irregular segment containing residues 1–33 and a small α-helix (residues 34–41). The linker segment 13–32 is essentially disordered in the electron density. In contrast, residues 1–12 are clearly visible in the electron-density map as they are artificially rigidified by a crystal contact to a neighbouring subunit mediated by Zn^{2+} ions (see §3.3). Therefore, we assume that in the cell the irregular segment is highly flex-

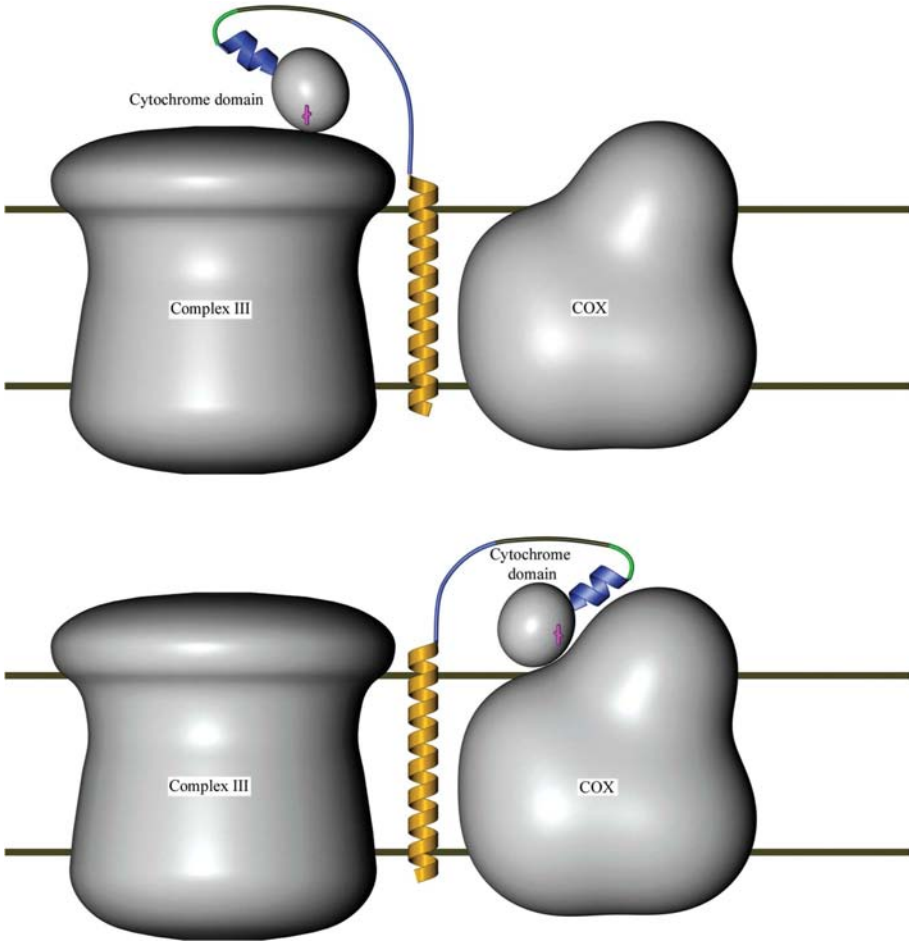

Figure 4
Schematic representation of c_{552} shuttling electrons between the bc_1 complex (complex III) and the cytochrome oxidase (COX), showing the interaction region with either cytochrome c_1 of complex III or the Cu_A domain of cytochrome oxidase.

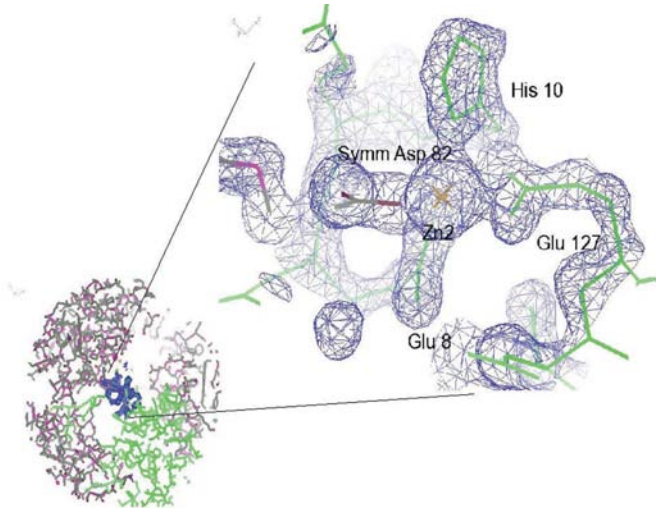

Figure 5
Schematic representation of cytochrome c_{552} (green) and its symmetry-related molecules (grey and pink). The electron-density map showing the coordination of one of the zinc ions (Zn2) by His10, Glu127 and Glu8 from cytochrome c_{552} and Asp82 from its symmetry-related molecule is highlighted. The space between the molecules shows that there is enough space for the disordered portion of the molecule. This figure was created with *Coot* (Emsley *et al.*, 2010).

ible as previously predicted by Berry & Trumpower (1985).

This linker region is endowed with a predominance of negatively charged residues consisting of seven glutamates and two aspartates (Fig. 2). The linker segment therefore appears to be well designed to prevent secondary-structure formation and attachment to the globular cytochrome *c* domain. This is also demonstrated by the fixed residues 1–12, which do not form a regular secondary structure and are only associated with the neighbouring cytochrome *c via* Zn^{2+} ions that link the negatively charged surfaces.

The high flexibility of segment 1–41 might be functionally important in this protein as it can be used as an arm to shuttle electrons between the bc_1 complex and cytochrome oxidase. Based on our structure, we propose a model for this process (Fig. 3). The small α-helix (residues 34–41) is distant from the haem-exposed region, which indicates that it does not interfere with electron transfer. The short helix 34–41 could play an important role in positioning the cytochrome *c* domain to interact favourably with its redox partner, which is necessary for effective electron transfer. Fig. 4 shows the proposed geometrical relation between the helix and the the interaction region of cytochrome oxidase.

3.3. Zinc-binding sites

The electron-density map revealed four strong spherical shaped peaks that were interpreted as Zn^{2+} ions because of the presence of $ZnSO_4$ in the crystallization buffer, which is essential for crystal formation, and because of the ligation pattern, which is typical of Zn^{2+} ions. Table 2 lists the zinc sites, their coordinating atoms and the distances between them. All four Zn^{2+} ions are endowed with a tetrahedral ligation shell containing at least one histidine and one glutamate ligand, which are considered to be essential features for Zn^{2+} ligation. This finding is also in agreement with previous reports. The other ligation sites are occupied by other proteinaceous ligands or by water molecules.

All of these zinc sites are located on the protein surface and mediate intermolecular interactions in the crystal lattice. Zn^{2+} is able to link negatively charged regions of two molecules which would otherwise repel each other and are therefore not appropriate for forming a crystal contact. However, Zn^{2+} appears to require a histidine side chain for complex formation. These Zn ions help to stabilize the N-terminal flexible loop by bridging its negatively charged residues with other symmetry-related molecules in the crystallographic unit cell (Fig. 5). On the other hand, the flexibility of the arm is useful for crystallization as it opens the possibility of positioning it where a Zn^{2+}-binding site can be formed.

Zn^{2+} binding allows the attachment of the negatively charged linker arm to the negatively charged globular domain, thereby causing rigidification.

Therefore, Zn^{2+} facilitates crystallization in two ways: by providing rigidity to the flexible loop by coordinating the negatively charged

residues from two different molecules and by enhancing the crystal contacts.

Zn^{2+} is therefore a good candidate for the successful crystallization of proteins with negative surface charges. It has long been known that divalent cations facilitate protein crystallization (McPherson, 1982, 1990). One well known example is Cd^{2+}. The role of cadmium has previously been demonstrated in the successful crystallization of many proteins (see, for example, Yao *et al.*, 1994; Nickitenko *et al.*, 1995; Trakhanov & Quiocho, 1995).

4. Conclusions

The interactions between the various components of the respiratory chain are short-lived, thus complicating their structural analysis. There are no cocrystals available for cytochrome c_{552} and its redox partners (complex III and IV) for analysis of the binding sites between them, which would be an interesting interaction study. Obtaining cocrystals of complex IV and cytochrome c_{552} or complex III and cytochrome c_{552} or the supercomplex (complex IV, complex III and cytochrome c_{552}) is a challenging but exciting task. It would also be interesting to analyze the structure of the full-length cytochrome c_{552}, which contains an additional membrane anchor, and to compare it with the structures of the soluble fragments. However, the existence of a flexible linker has so far precluded crystallization.

We thank the beamline staff of X10SA (Swiss Light Source, Paul Scherrer Institute, Villigen) for their excellent support. We thank Dr Meitian Wang for help at SLS. The Deutsche Forschungsgemeinschaft (SFB 472) and the Max-Planck-Gesellschaft supported this work. We thank Paolo Lastrico for his help in producing excellent pictures for publication.

References

Berry, E. A. & Trumpower, B. L. (1985). *J. Biol. Chem.* **260**, 2458–2467.
Brünger, A. T., Adams, P. D., Clore, G. M., DeLano, W. L., Gros, P., Grosse-Kunstleve, R. W., Jiang, J.-S., Kuszewski, J., Nilges, M., Pannu, N. S., Read, R. J., Rice, L. M., Simonson, T. & Warren, G. L. (1998). *Acta Cryst.* D**54**, 905–921.
Bushnell, W. G., Louie, V. G. & Brayer, D. G. (1990). *J. Mol. Biol.* **214**, 585–595.
DeLano, W. L. (2008). *PyMOL Molecular Viewer*. DeLano Scientific LLC, Palo Alto, California, USA. http://www.pymol.org.
Emsley, P., Lohkamp, B., Scott, W. G. & Cowtan, K. (2010). *Acta Cryst.* D**66**, 486–501.
Engh, R. A. & Huber, R. (1991). *Acta Cryst.* A**47**, 392–400.
Harrenga, A., Reincke, B., Rüterjans, H., Ludwig, B. & Michel, H. (2000). *J. Mol. Biol.* **295**, 667–678.
Hooft, R. W., Vriend, G., Sander, C. & Abola, E. E. (1996). *Nature (London)*, **381**, 272.
Janzon, J., Yuan, Q., Malatesta, F., Hellwig, P., Ludwig, B., Durham, B. & Millett, F. (2008). *Biochemistry*, **47**, 12974–12984.
Kissinger, C. R., Gehlhaar, D. K. & Fogel, D. B. (1999). *Acta Cryst.* D**55**, 484–491.
Laskowski, R. A., MacArthur, M. W., Moss, D. S. & Thornton, J. M. (1993). *J. Appl. Cryst.* **26**, 283–291.
McPherson, A. (1982). *Preparation and Analysis of Protein Crystals*. New York: John Wiley & Sons.
McPherson, A. (1990). *Eur. J. Biochem.* **189**, 1–23.
McRee, D. E. (1993). *Practical Protein Crystallography*. San Diego: Academic Press.
Murshudov, G. N., Vagin, A. A. & Dodson, E. J. (1997). *Acta Cryst.* D**53**, 240–255.
Nickitenko, A. V., Trakhanov, S. & Quiocho, F. A. (1995). *Biochemistry*, **34**, 16585–19595.
Otwinowski, Z. & Minor, W. (1997). *Methods Enzymol.* **276**, 307–326.
Reincke, B., Thöny-Meyer, L., Dannehl, C., Odenwald, A., Aidim, M., Witt, H., Rüterjans, H. & Ludwig, B. (1999). *Biochim. Biophys. Acta*, **1411**, 114–120.
Trakhanov, S. & Quiocho, F. A. (1995). *Protein Sci.* **4**, 1914–1919.
Turba, A., Jetzek, M. & Ludwig, B. (1995). *Eur. J. Biochem.* **231**, 259–265.
Witt, H., Malatesta, F., Nicoletti, F., Brunori, M. & Ludwig, B. (1998). *J. Biol. Chem.* **273**, 5132–5136.
Yao, N., Trakhanov, S. & Quiocho, F. A. (1994). *Biochemistry*, **33**, 4769–4779.
Zhen, Y., Hoganson, C. W., Babcock, G. T. & Ferguson-Miller, S. (1999). *J. Biol. Chem.* **274**, 38032–38041.